



Dynamic functional connectivity in temporal lobe epilepsy: a graph theoretical and machine learning approach

Alireza Fallahi¹ · Mohammad Pooyan¹ · Nastaran Lotfi² · Fatemeh Baniasad^{3,6} · Leili Tapak^{4,5} · Neda Mohammadi-Mobarakeh^{3,6} · Seyed Sohrab Hashemi-Fesharaki⁷ · Jafar Mehvari-Habibabadi⁸ · Mohammad Reza Ay^{3,6} · Mohammad-Reza Nazem-Zadeh^{3,6} 

Received: 11 July 2020 / Accepted: 23 September 2020

© Fondazione Società Italiana di Neurologia 2020

Abstract

Purpose Functional magnetic resonance imaging (fMRI) in resting state can be used to evaluate the functional organization of the human brain in the absence of any task or stimulus. The functional connectivity (FC) has non-stationary nature and consented to be varying over time. By considering the dynamic characteristics of the FC and using graph theoretical analysis and a machine learning approach, we aim to identify the laterality in cases of temporal lobe epilepsy (TLE).

Methods Six global graph measures are extracted from static and dynamic functional connectivity matrices using fMRI data of 35 unilateral TLE subjects. Alterations in the time trend of the graph measures are quantified. The random forest (RF) method is used for the determination of feature importance and selection of dynamic graph features including mean, variance, skewness, kurtosis, and Shannon entropy. The selected features are used in the support vector machine (SVM) classifier to identify the left and right epileptogenic sides in patients with TLE.

Results Our results for the performance of SVM demonstrate that the utility of dynamic features improves the classification outcome in terms of accuracy (88.5% for dynamic features compared with 82% for static features). Selecting the best dynamic features also elevates the accuracy to 91.5%.

Conclusion Accounting for the non-stationary characteristics of functional connectivity, dynamic connectivity analysis of graph measures along with machine learning approach can identify the temporal trend of some specific network features. These network features may be used as potential imaging markers in determining the epileptogenic hemisphere in patients with TLE.

Keywords Dynamic functional connectivity · Temporal lobe epilepsy · Graph theory · Lateralization · Machine learning

Introduction

Temporal lobe epilepsy (TLE) is the most frequent type of pharmaco-resistant focal epilepsy in adults accountable for surgical treatment. However, due to a lack of clear localizing the

seizer source, surgery cannot be performed in about 30% of TLE patients [1]. In standard presurgical evaluation protocols, video-EEG and high-resolution MRI play a critical role [2]. Functional connectivity based on functional MRI (fMRI) may provide additional useful information for the purpose of lateralization.

✉ Mohammad-Reza Nazem-Zadeh
mnazemzadeh@tums.ac.ir

Alireza Fallahi
fallahi@hut.ac.ir

Mohammad Pooyan
pooyan@shahed.ac.ir

Fatemeh Baniasad
pooneh.baniasad@gmail.com

Leili Tapak
l.tapak@umsha.ac.ir

Neda Mohammadi-Mobarakeh
nedamohammadi157@gmail.com

Seyed Sohrab Hashemi-Fesharaki
shfesharaki@yahoo.com

Jafar Mehvari-Habibabadi
dr.mehvari@hotmail.com

Mohammad Reza Ay
mohammadreza_ay@tums.ac.ir

Extended author information available on the last page of the article

Functional and structural neuroimaging analyses have supported the theory that TLE is a disorder which may affect brain regions and alter networks in temporal lobe and beyond [3–9].

Recent studies show that the patterns of functional connectivity may be different between left TLE (L-TLE) and right TLE (R-TLE), including redistribution of global functional activation in L-TLE and functional impairments in R-TLE [10–14]. Default mode network (DMN) and motor network (MN) are among subcortical networks where functional alterations have been evidenced [15, 16].

The graph-based connectivity analysis is a powerful quantitative method for explaining the topological architecture of complex brain networks. Network abnormalities in terms of functional connectivity using graph theoretical metrics may be served as markers for clinical diagnostic and also disease staging estimation [17, 18]. The efficiency, clustering, modularity, and small-worldness are among network metrics that extract topological properties of brain networks [19, 20].

Despite a large amount of research using graph-based connectivity analysis in resting state, the majority of studies are based on temporal stationarity assumption of the functional interaction between blood-oxygen-level-dependent (BOLD) signals. However, recent studies increasingly have shown that functional connectivity between brain regions is inherently non-stationary and evidenced to be varying over time and associated with the cognitive states [21, 22]. Functional connectivity has been shown to be dynamic and varied during scan time [23], which may be appropriately modeled by the first-order temporal dynamics. Investigating resting-state brain topology from a dynamic perspective is a relatively new concept and still under the debate, it reflects the functional network configuration overlying on a steady platform of anatomy [24, 25].

Recently, some studies have reported discrepant results provided by graph theory for functional connectivity [26, 27]. For instance, an altering trend in clustering coefficient and characteristic path length has been reported in patients with epilepsy compared with controls [3, 28]. In addition, the temporal instability in some topological features inspires the researchers to obtain the topology of functional network settings [29]. Adopting a dynamic approach in graph-based

analysis of the network topology may address inconsistencies in the previous studies.

In this study, we exploited the clustering coefficients and centrality-based graph measures including degree centrality, betweenness centrality, closeness centrality, and page rank, as well as node neighbor's degree as a new graph measure. We used these measures for analyzing resting-state fMRI and characterizing the differences in static and dynamic functional connectivity between the L-TLE and R-TLE patients. Using a machine learning approach, we also analyzed these graph measures for characterizing nodal level differences between L-TLE and R-TLE in resting-state functional networks.

Materials and methods

Subjects

We studied 35 unilateral patients with left or right TLE (see Table 1 for the patient characteristics). The study was approved by the Institutional Review Board of Tehran University of Medical Sciences. Patients with disabling cognitive impairment or with other neurological diseases were excluded beforehand. Twenty-one cases were L-TLE and 14 cases were R-TLE.

Image acquisition

MRI images were acquired on a 3-T scanner (Siemens Prisma, Erlangen, Germany) at the Iranian National Brain Mapping Laboratory (NMBL). Using an EPI resting-state fMRI protocol, 330 functional volumes were acquired with the imaging parameters of TR/TE = 3000/30 ms, flip angle = 90°, acquisition matrix = 64 × 64, and the slice thickness = 2.4 mm in 16.5 min, while the patients were instructed to relax with their eyes closed and think nothing in particular. Using an MP-RAGE protocol, T1-weighted structural scans were acquired for clinical diagnostic purposes, with the imaging parameters of TR/TE = 1840/3.47 ms, acquisition matrix = 256 × 256, and slice thickness = 1.0 mm.

Table 1 Participant characteristics

Characteristic	Left TLE	Right TLE	<i>P</i> value
Sample size	21	14	-
Sex (M/F)	10/11	8/6	0.73 [‡]
Age (years), mean ± STD [range]	31.9 ± 8.2 [17–54]	26.8 ± 6.2 [17–36]	0.059*
Onset age (years), mean ± STD [range]	10.8 ± 8.2 [0.5–29]	9.4 ± 9.4 [0.5–28]	0.6*

[‡]Fisher exact test

*Two-sample *t* test

Image preprocessing

DPARSF 4.3 and REST toolboxes (<http://rfmri.org/dpabi>) [30] were performed for preprocessing of the resting-state fMRI data. For each subject, the first 10 time points were removed. The remaining 320 volumes were first corrected for the time difference between slices and then realigned to the middle volume for head motion correction (no participant had head motion no greater than 3 mm or 3°). Using the normalization parameters estimated by the T1 structural image, the realigned functional volumes with a voxel size of (3,3,3) were spatially normalized to the Montreal Neurological Institute (MNI) space. Then, using a Gaussian kernel (FWHM = 8 mm), the dataset was smoothed, linearly detrended, and temporally filtered (0.01–0.08 Hz) to decrease the effect of low-frequency drifts. Using Automated Anatomical Labeling (AAL) atlas [31], the volumes were segmented into 90 anatomical regions of interest (ROIs) to extract the ROI time series. The mean time series of all voxels within the ROIs were used for the connectivity analysis.

Connectivity analysis and graph theory measures

We calculated functional connectivity using Pearson's correlation coefficient between each pair of ROI time series representing brain regional activity (Eq. 1).

$$\rho_{X,Y} = \frac{E[(X-\mu_X)(Y-\mu_Y)]}{\sigma_X\sigma_Y} \quad (1)$$

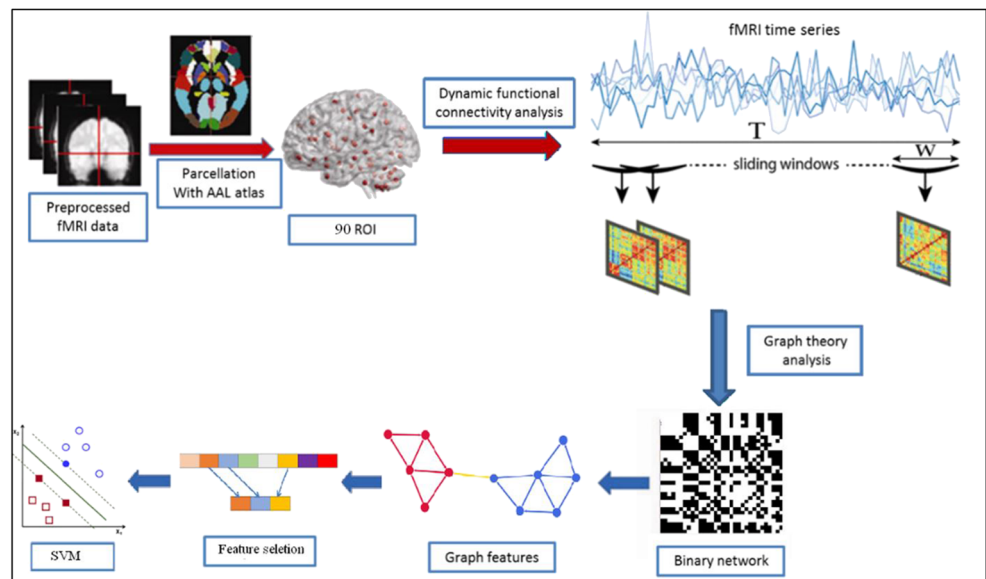
where μ_X and μ_Y are the mean and σ_X and σ_Y are the standard deviations of the signals X and Y, respectively, and $E[.]$ is the expectation operator. Pearson's correlation coefficient result is

a symmetric adjacency matrix for each patient. For dynamic functional connectivity, the time-varying correlation analysis between brain regions was performed while sliding time windows, characterized by the length W (from time $t = 1$ to time $t = W$). The same calculations were then repeated in the shifted window by a temporal lag L , over the time interval $[1 + L, W + L]$. This process was repeated until the window spanned the end part of the time courses, to eventually obtain a connectivity time course (Fig. 1). Window sizes of 30–60 s have been suggested in previous works to capture the fluctuations in the resting-state functional connectivity [32] with only small effects on capturing the effective functional dynamics [33]. We considered $W = 30$ s for window size, with a lag $L = 6$ s in total scan time $T = 16$ m (considering removal of the first 10 points). Static functional connectivity was also calculated to compare its results with that of dynamic connectivity.

Negative correlations of functional connectivity matrix were set to 0 to improve the reliability of graph theory measures [34]. Furthermore, some of the unweighted and undirected links were removed by thresholding the adjacency matrix. Since there is no definitive agreement on the threshold selection method, based on previous studies [35, 36], a set of proportional thresholds was investigated over a range from 0.5 to 0.9 corresponding to a number of edges from 2520 to 1420, respectively. For example, a proportional threshold of 0.9 indicates that the 10% strongest connections are retained.

Various brain network topology measures such as nodal and global characteristic path length, centrality, efficiency, and small-worldness have been investigated in previous studies [3, 27, 37, 38]. Centrality metrics represent how information is integrated and communicated through regions in the brain network. Unlike independent component analysis (ICA) or seed-based approaches, centrality metrics account for each region's relationship with the entire functional connectivity,

Fig. 1 The concept of dynamic functional connectivity analysis using the sliding window technique



not just its relation to individual regions; therefore, they explain global sensitivity [39, 40]. As such, we opted to focus on centrality properties to capture the complexity of the fMRI functional connectivity. Centrality metrics including degree centrality, betweenness centrality, closeness centrality, and page rank have been previously investigated in the literature. We also used node neighbor's degree as another centrality metric, which is a method for measuring dependencies between degrees of neighbor nodes in a graph and represented as follows:

$$C_N(i) = \frac{1}{|N(i)|} \sum_{j \in N(i)} k_j \quad (2)$$

where $N(i)$ are the neighbors of the nodes i and k_j is the degree of the node j belonging to $N(i)$.

The clustering coefficient has been used as one of the common and informative graph metrics in functional connectivity analysis [41–43]. Represented graph measures were examined in a nodal level. Python NetworkX (Python library for studying graphs and networks) was used for the calculation of graph theoretical parameters.

Statistical analysis

We used a multilevel mixed effects linear regression model to determine the time trends. To this end, a regression coefficient was considered for the time element in the model. Negative and positive values of the regression coefficients indicated decreasing and increasing trends, respectively. The same method was applied for the statistical analysis using R software on a significant difference between L-TLE and R-TLE groups ($P < 0.05$).

Feature selection and classification

In the third step, the right and left TLE patients were classified using the graph features. Feature extraction and selection for static and dynamic analyses are explained as follows.

Static analysis

We represented graph properties of all 90 nodes for each subject. We considered 6 feature categories corresponding to 6 graph measures. Each feature category contained 90 values corresponding to the related nodes. We used random forest (RF) method for feature selection in each feature category, which is an ensemble method using a large number of random decision trees [44]. In RF, random subsets of the observations (bootstrapped sampling) and candidate variables are used for creating each of the trees. In the current study, in each feature category over all subjects, RF method was repeated 100 times and nodes were ranked due to their average importance. Top 5

to 40 high ranked nodes (with a step of 5) were selected for each feature category.

Dynamic analysis

In dynamic analysis, in addition to the burden of the high dimensionality in the spatial domain and feature space, the time window is an additional “curse of dimensionality.” We calculated the following attributes for dynamic connectivity: mean, variance, skewness, kurtosis, and Shannon entropy across all time windows for each of the 6 nodal graph measures. In dynamic analysis, the total number of features category was set to 30 (5 time features \times 6 graph features), to each we assigned 90 nodes as a single feature. The RF method ranked the nodes in each feature category over all subjects; the top 5 to 40 high ranked nodes (with a step of 5 numbers of selected nodes) were subsequently selected for classification.

Classification

Support vector machine (SVM) classifier was employed for classification with a quadratic kernel. Leave-one-out cross-validation (LOOCV) approach was used for training and testing of SVM classification. For each measure, a subject data was used for testing, and the remaining was used for training. The performance of the classifier was assessed using the classification accuracy and receiver operating characteristic (ROC) curves. MATLAB R2018b was used for SVM classification, ROC, and RF method analysis.

For both static and dynamic feature categories, we applied the SVM classifier using the top 5 to 40 high ranked nodes (with a step size of 5) separately. For the number of nodes with the best classification results, we applied four levels of classification accuracy threshold (0.5, 0.6, 0.7, and 0.8) for features categories. The ones with an accuracy higher than a specific threshold were selected as the best feature categories associated with it. Then, we applied the classification again using the selected feature categories for different threshold values. Finally, we considered the feature categories with the most classification accuracy as the final selected feature categories.

Results

The application of a high threshold for the graph binarization would cause a sparse connectivity matrix with a few connections between the nodes. On the other hand, a low threshold would cause an over connection between the nodes and the network to become almost a regular lattice. Given these, we chose a medium threshold of 0.8 as proportional thresholding for preserving small-worldness property of real functional networks in the brain.

Statistical analysis results

The statistical results of static functional connectivity in Table 2 show that degree and closeness centralities in L-TLE patients were significantly larger than those in R-TLE patients ($P < 0.05$). In addition, betweenness centrality in L-TLE patients was significantly smaller than that in R-TLE patients ($P < 0.05$). No significant difference between the two groups was found for any of clustering coefficient, node neighbor's degree, or page rank features.

Dynamic functional connectivity, on the other hand, suggested that the clustering coefficient, betweenness centrality, and node neighbor's degree measures in L-TLE patients were significantly smaller compared with R-TLE patients ($P < 0.05$). Furthermore, the degree centrality and closeness centrality metrics were significantly larger in L-TLE patients compared with R-TLE patients ($P < 0.05$). Using the page rank feature, we did not show any significant difference between the two TLE groups.

Time trend of graph measures

The alternation of each graph measure during imaging time was investigated. As presented in Table 3, the clustering coefficient showed a decrease in L-TLE and an increase in R-TLE patients. Also, our results showed that the degree centrality, node neighbor's degree, and closeness centrality measures were decreased and the page rank was increased in both L-TLE and R-TLE patients. The betweenness centrality measure was decreased in L-TLE and increased in R-TLE patients during imaging time

Classification result

There were 540 candidate features (6 feature categories in 90 nodes) in static analysis. Figure 2 shows the result of classification accuracy for 5 to 40 most important nodes selected in each graph measure. The page rank and then the node neighbor's degree showed superior accuracy compared with other graph measures. There were also 2700 candidate features (30 feature categories in 90 nodes) in dynamic analysis. Figure 3 shows the result of classification accuracy for 5 to 40 most important nodes selected in each new feature category.

Table 2 Result of static and dynamic graph characteristics analysis

Graph measures	Clustering coefficient	Degree centrality	Betweenness centrality	Node neighbor's degree	Closeness centrality	Page rank
Static	L = R	L > R	L < R	L = R	L > R	L = R
Dynamic	L < R	L > R	L < R	L < R	L > R	L = R

Figure 4a shows the classification accuracy for the 5 to 40 most important nodes among all candidate feature categories. As can be observed, the 15 selected nodes have the best performance in static and dynamic analyses with 82.0% and 88.5% accuracy, respectively. Figure 4b shows the result of classification using the selected feature categories related to multiple thresholds on accuracy values using 15 selected nodes. It shows that the static analysis using feature categories with accuracy higher than 0.6 has led to the highest performance. Likewise, dynamic analysis using feature categories with accuracy higher than 0.7 achieved the highest performance. Therefore, static analysis with 3 feature categories, namely the clustering coefficient, node neighbor's degree, and the page rank, was the best-selected feature categories with the highest performance. For dynamic analysis, on the other hand, the skewness in clustering coefficient (CC-S), kurtosis in clustering coefficient (CC-K), entropy in clustering coefficient (CC-SE), mean in degree centrality (DC-M), entropy in betweenness centrality (BC-SE), and entropy in node neighbor's degree (NND-SE) were the top 6 dynamic feature categories with the highest performance.

Figure 4c shows the result of classification performance using the best-selected feature categories (3 feature categories in static and 6 feature categories in dynamic analyses, respectively) using the 15 selected nodes. As can be seen, the best accuracies for the static and dynamic analyses were 88.0% and 91.5%, respectively.

The ROC curves of the classifiers in static and dynamic analyses using all feature categories of the top 15 ranked nodes (best number of selected nodes) are shown in Fig. 5. The area under the ROC (AUC) for the SVM classifiers based on the static and dynamic features was calculated as 86% and 91%, respectively. The AAL ROIs and the relative importance of the top-five ranked nodes in static and dynamic selected feature categories are shown in Tables 4 and 5.

Discussion

In this paper, we compared the analyses of static and dynamic functional connectivity for the application of lateralizing TLE patients. We proposed graph-based quantitative metrics for the determination of the laterality for the left and right TLE patients using both static and dynamic analyses. The feature

Table 3 Time trend of dynamic graph characteristics

Graph measures	Clustering coefficient		Degree centrality		Betweenness centrality		Node neighbor's degree		Closeness centrality		Page rank	
	Left	Right	Left	Right	Left	Right	Left	Right	Left	Right	Left	Right
Time trend	↓	↑	↓	↓	↓	↑	↓	↓	↓	↓	↑	↑

↑ represents increase and ↓ represents a decrease

space of graph measures of each time window in the dynamic analysis was converted to statistical representation to overcome the “curse of dimensionality.” A feature selection method based on RF was developed to deal with the problem of over-fitting. All findings demonstrated the importance of the dynamic analysis approach, in particular, the clustering coefficient and Shannon entropy measures, in the development of biomarkers for TLE lateralization.

Based on the static analysis, neither the clustering coefficient nor the node neighbor's degree and page rank showed a significant difference between the two TLE groups using statistical analysis. However, based on dynamic connectivity analysis, except for page rank, they all showed significant differences. Therefore, dynamic functional connectivity analysis was demonstrated as a more powerful technique to characterize the brain network and its laterality in cases of TLE.

The degree centrality, betweenness centrality, and closeness centrality are common graph measures for fMRI connectivity analysis [37, 39, 45]. The page rank also is a variant of eigenvector centrality that has been used in brain connectivity and epilepsy cases in previous studies [27, 46, 47]. The worldwide web, as well as the human brain, would exhibit small-world properties suggesting that an algorithm that is quite effective as a part of a search engine may also be efficient in analyzing network properties in the human brain. The page rank did not make a significant difference in left TLE and right TLE groups based on our statistical analysis both in static and

dynamic approaches, but this graph measure provided the highest classification rate in the static analysis which can be due to the statistical analysis applies a linear method for comparing two groups, but an SVM classifier applies a nonlinear kernel for separating two groups. These results show that the page rank is a complex feature suitable for connectivity analysis in the brain as a complex system.

Our classification results based on the static analysis showed that the node neighbor's degree has superior accuracy compared with the degree centrality, betweenness centrality, and closeness centrality and also this graph metric is one of the selected feature categories in dynamic analysis, stressing that the node neighbor's degree can be used as a robust feature for lateralization of TLE. The clustering coefficient is another most commonly used graph metrics in functional connectivity analysis in TLE [36, 43, 48, 49]. This graphic metric was one of the three selected feature categories in static analysis and based on the dynamic analysis our results showed that the clustering coefficient has a superior role compared to the degree centrality, betweenness centrality, and the node neighbor's degree in the selection of the best feature categories. This suggests that the clustering coefficient is an appropriate graph measure in dynamic analysis for TLE lateralization. Our analysis of the time trend of dynamic graph metrics showed that the clustering coefficient and betweenness centrality metrics can lateralize the left and right TLE patients, which emphasizes the advantage of the dynamic over the static analysis.

Fig. 2 Accuracy of classification using static feature categories for the different number of selected nodes. SN, selected nodes; CC, clustering coefficient; DC, degree centrality; BC, betweenness centrality; NND, node neighbor's degree; CNS, closeness centrality; PR, page rank

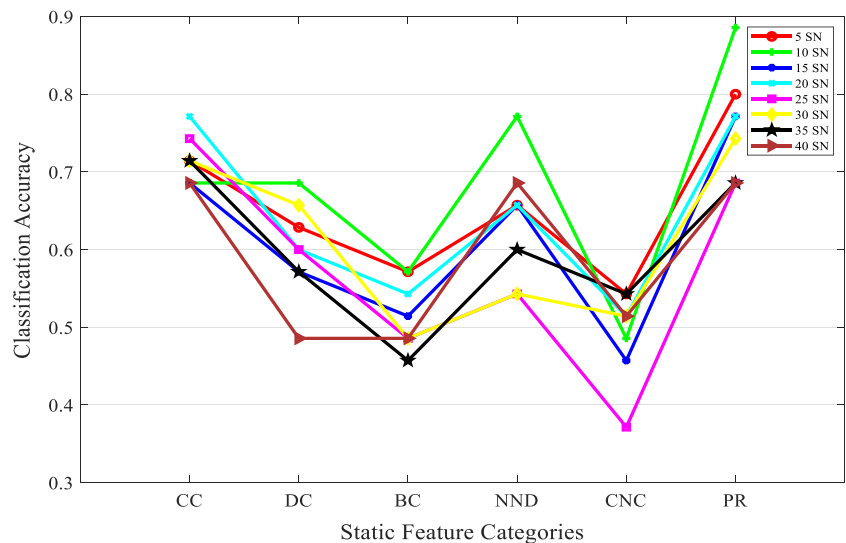


Fig. 3 Accuracy of classification using dynamic feature categories for the different number of selected nodes. SN, selected nodes; CC, clustering coefficient; DC, degree centrality; BC, betweenness centrality; NND, node neighbor's degree; CNS, closeness centrality; PR, page rank; M, mean; V, variance; S, skewness; K, kurtosis; SE, Shannon entropy

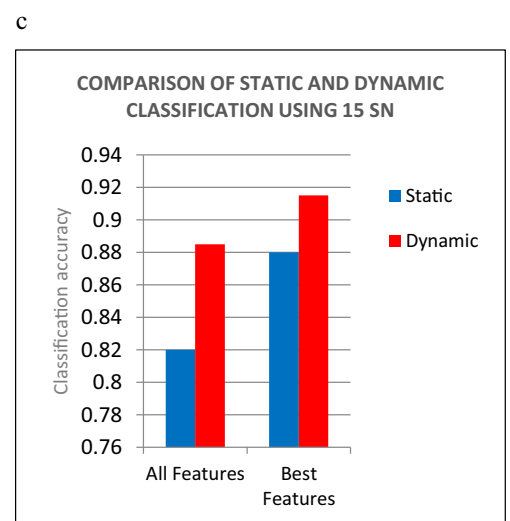
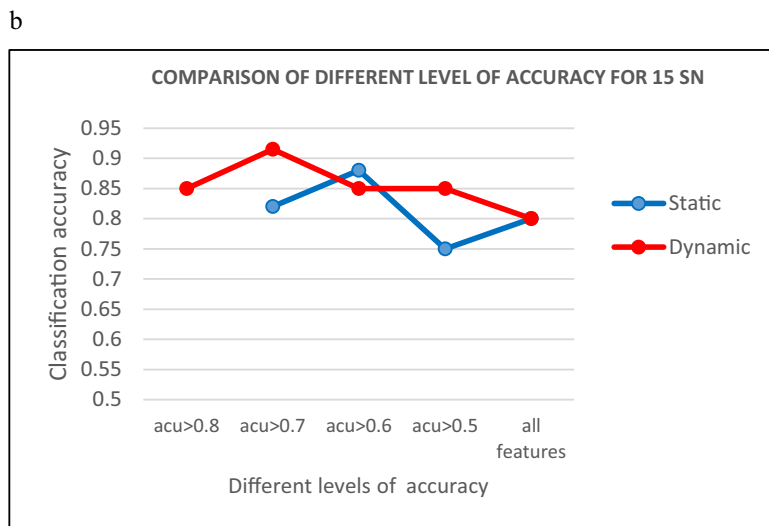
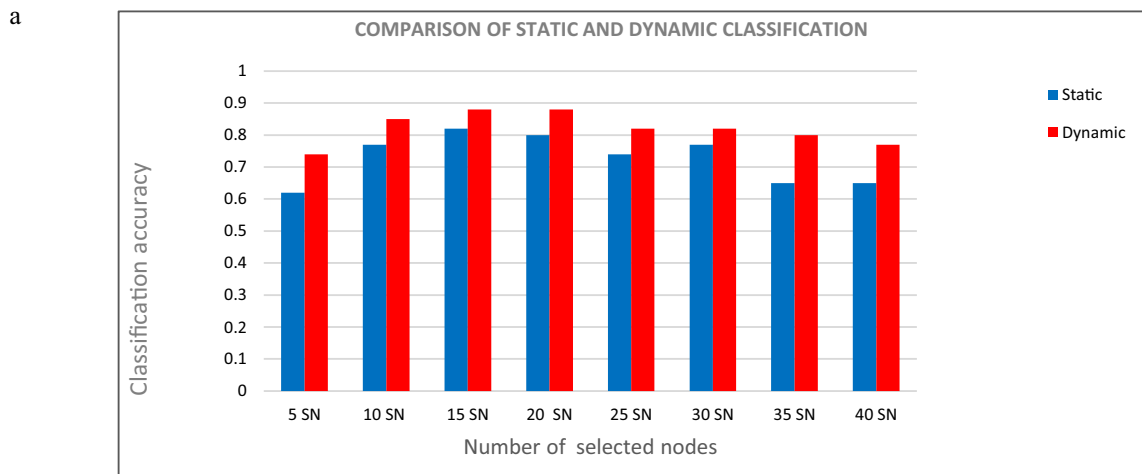
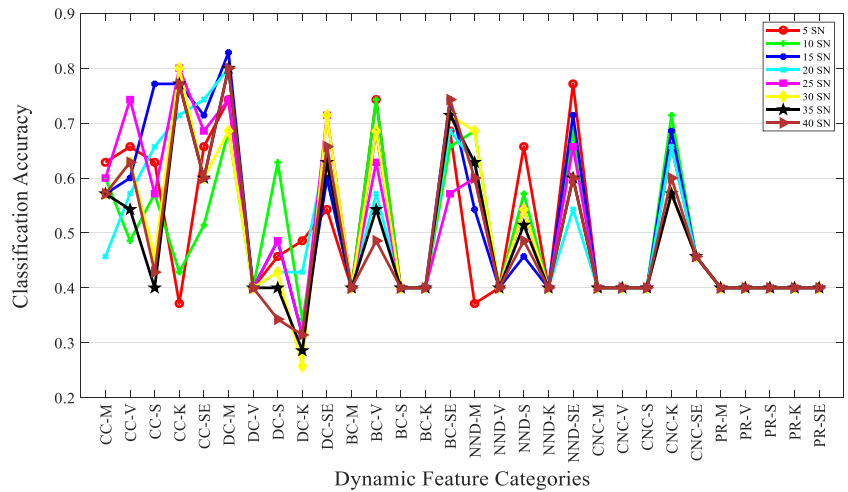


Fig. 4 Comparison of static and dynamic classification accuracy using all and best feature categories. **a** Classification accuracy for the 5 to 40 most important nodes using all feature categories. Note that the classifier based on the 15 selected nodes provides the best performance in static and dynamic analyses with an accuracy of 82.0% and 88.5%, respectively. **b** Result of classification using the selected feature categories associated

with multiple thresholds on accuracy values using 15 selected nodes. **c** Classification performance using the best of selected feature categories (3 features in static and 6 features in dynamic analysis) in the 15 selected nodes. This figure shows that the best achieved accuracies in the static and dynamic analyses were 88.0% and 91.5%, respectively

Table 4 The top 5 ranked nodes in the clustering coefficient, node neighbor's degree, and page rank in the static connectivity analysis

Nodal rank	Clustering coefficient	Node neighbor's degree	Page rank
1	PCG.R	REC.L	MOG.R
2	DCG.L	ANG.R	CUN.R
3	PCUN.R	IOG.L	IOG.L
4	ORBinf.L	SPG.L	PreCG.R
5	PUT.L	REC.R	SFGdor.L

PCG, posterior cingulate gyrus; *DCG*, median cingulated gyrus; *PCUN*, precuneus; *ORBinf*, inferior frontal gyrus; *PUT*, putamen; *REC*, gyrus rectus; *ANG*, angular gyrus; *IOG*, inferior occipital gyrus; *SPG*, superior parietal gyrus; *MOG*, middle occipital gyrus; *CUN*, cuneus; *PreCG*, precentral gyrus; *SFGdor*, superior frontal gyrus; *L*, left hemisphere; *R*, right hemisphere

Most of the previous studies using the functional connectivity and machine learning approaches for lateralization of TLE concentrate merely on the static functional connectivity or time series for connectivity analysis [3, 37, 38, 50–52]. Extracting a large amount of information from fMRI time series is one of the main advantages of the dynamic functional connectivity analysis, which may be dismissed in a static approach. However, the poor interpretability and noisiness of the raw time series have restricted the direct usage of dynamic estimates.

The importance of first- and second-order statistics in extracting features from dynamic graphic features in understated [53]. Our proposed approach was novel in the sense that we investigated higher-order characteristic information from the graph measures in dynamic analysis, proven to be more resistant to noise and interpretability in machine learning approaches. Our results were in agreement with other studies that applied higher-order statistics as a second level feature extraction in dynamic connectivity analysis [54]. We showed that the Shannon entropy measure may have more promising

outcomes in the classification task. This could be due to the complexity of this feature over the mean, variance, skewness, and kurtosis, which can capture more information content from dynamic functional connectivity.

Our examination of multiple importance scores showed that restricting the static and dynamic functional connectivity assessments merely to the 3 and 6 best feature categories, respectively, may increase the accuracy of machine learning algorithms.

Previous studies have found that static functional connectivity and its fluctuation over time specified abnormal functional avidities in neurological disorders such as temporal lobe epilepsy [3, 55–57]. Our results show that dynamic features are more sensitive in the detection of abnormal epileptic avidities compared with the static features. These findings are summarized as follows based on top-ranked nodes using best-selected feature categories in static and dynamic analysis.

In static analysis, the node neighbor's degree of the left and right gyrus rectus were within the top-ranked nodes. The gyrus rectus is a region with increased connectivity manifested during interictal spikes [58]. We also observed that the clustering coefficient in the right posterior cingulate gyrus and right precuneus and the page rank in the left superior frontal gyrus were other top-ranked nodes. Previous studies have also reported these regions as practicable markers for the lateralization of TLE patients [8].

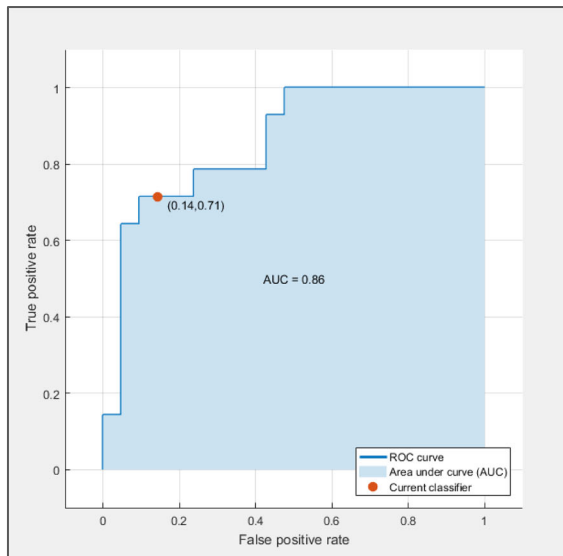
Frontal regions were also previously reported as alternate regions in TLE [3, 59]. Based on our findings, the frontal regions including the inferior frontal gyrus (by both static and dynamic analyses) were among the top-ranked nodes. Our findings based on static analysis, in agreement with the previous studies reporting the impaired networks in patients with TLE [60], showed that the following regions constitute the top-ranked nodes in the classification of L-TLE and R-TLE within the specific functional networks:

Table 5 The top five ranked nodes for the six best dynamic features

Nodal rank	CC_S	CC-K	CC_SE	DC-M	BC-SE	NND-SE
1	FFG.L	LING.R	HES.L	HIP.L	MTG.L	ROL.R
2	ORBsup.R	REC.R	TPOsup.R	PCL.R	ORBsupmed.L	PCUN.R
3	CUN.L	PHG.R	AMYG.L	IOG.L	MOG.L	FFG.L
4	ORBinf.L	OLF.L	PALL	PCUN.L	IFGtriang.R	ITG.R
5	HIP.R	AMYG.R	ORBsup.L	IPL.R	IPL.R	TPOmid.R

CC-S, skewness of clustering coefficient; *CC-K*, kurtosis of clustering coefficient; *CC-SE*, Shannon entropy of clustering coefficient; *DC-M*, mean of degree centrality; *BC-SE*, Shannon entropy of betweenness centrality; *NND-SE*, Shannon entropy of node neighbor's degree; *LING*, lingual gyrus; *REC*, gyrus rectus; *PHG*, parahippocampal gyrus; *OLF*, olfactory cortex; *AMYG*, amygdala; *HIP*, hippocampus; *PCL*, paracentral lobule; *IOG*, inferior occipital gyrus; *PCUN*, precuneus; *FFG*, fusiform gyrus; *ORBsupmed*, superior medial frontal gyrus; *MTG*, middle temporal gyrus; *MOG*, middle occipital gyrus; *IFGtriang*, inferior triangular frontal gyrus; *IPL*, inferior parietal gyrus; *ROL*, Rolandic operculum; *ITG*, inferior temporal gyrus; *TPOmid*, middle temporal gyrus; *ORBinf*, inferior orbitofrontal gyrus; *ORBsup*, superior orbitofrontal gyrus; *CUN*, cuneus; *HES*, Heschl gyrus; *TPOsup*, superior temporal gyrus; *AMYG*, amygdala; *PAL*, pallidum; *L*, left hemisphere; *R*, right hemisphere

a ROC for static connectivity analysis



b ROC for dynamic connectivity analysis

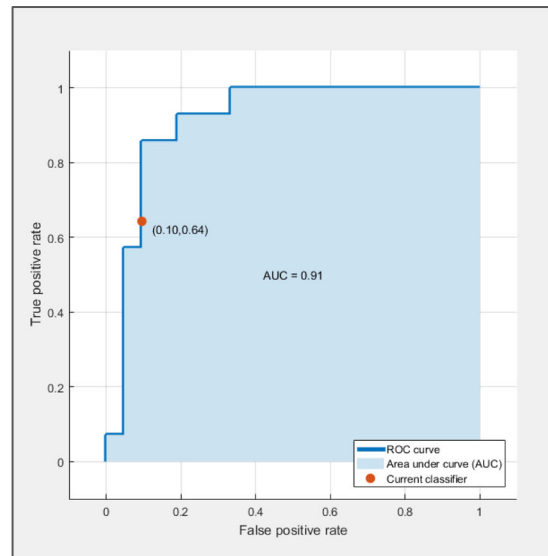


Fig. 5 The receiver operating characteristic curves (ROCs) for the classification of patients with R-TLE and L-TLE using the top 15 ranked nodes in the static and dynamic connectivity analyses. **a** The

area under the ROC (AUC) was 86% when all static feature categories were used for the classification. **b** The AUC was 91% when all dynamic feature categories were used for the classification

1. The clustering coefficient of the left median cingulate and the node neighbor's degree of the angular gyrus in the default mode network.
2. The page rank of the right cuneus and the right middle occipital gyrus; and the page rank and node neighbor's degree of the left inferior occipital gyrus in the visual network.
3. The node neighbor's degree of the left superior parietal and the page rank of the right precentral gyri in the somatomotor network.
4. The clustering coefficient of the right posterior cingulate gyrus and the left inferior orbitofrontal gyrus in the limbic network [3].
3. The mean of degree centrality in the right paracentral lobule in the somatomotor network
4. The Shannon entropy of betweenness centrality in the right inferior frontal gyrus in the attention network [60].
5. The skewness of clustering coefficient in the left inferior orbitofrontal gyrus and left fusiform gyrus; entropy of clustering coefficient in the right superior temporal gyrus; the entropy of node neighbor degree in the left fusiform gyrus in limbic Network [3].

In concordance with previous reports, our dynamic analysis found the top-ranked nodes in the following regions that can distinguish L-TLE and R-TLE withing the specific functional networks:

1. The mean of degree centrality and the Shannon entropy of betweenness centrality in the right inferior parietal, the Shannon entropy of node neighbor's degree in the right middle temporal gyrus, the skewness of clustering coefficient in the right superior frontal gyrus, and the Shannon entropy of clustering coefficient in the left superior frontal gyrus in default mode network
2. The Shannon entropy of clustering coefficient in left cuneus, the mean of degree centrality in the left inferior occipital gyrus, and the Shannon entropy of betweenness centrality in the left middle occipital gyrus in the visual network

Hippocampus and parahippocampal gyrus are among the temporal regions altered in TLE [3, 53, 61–64]. Our findings showed that left and right hippocampi would undergo alterations in the mean of degree centrality and skewness of the clustering coefficient, respectively. Furthermore, the right parahippocampal gyrus underwent changes in kurtosis of the clustering coefficient, which altogether make the top-ranked nodes in dynamic analysis. Our results evidenced that the left amygdala in the entropy of the clustering coefficient was one of the top-ranked nodes in the dynamic analysis and supported the previous findings that the amygdala may undergo changes in TLE [12, 63, 65]. These findings showed that the dynamic analysis could demonstrate more distinguishing regions in terms of laterality, compared with the static analysis.

Our study had several limitations. First, our sample size was relatively small (35 TLE cases), for which our findings need to be validated using a larger sample size. Another limitation is that healthy control subjects were not included in our study. Previous studies showed a wide range of TLE alterations in brain functional networks between the normal group and TLE subjects, some of which are similar in both left and

right TLE groups, yet different from the control healthy group and were not examined in our study. Recruiting control subjects in a future study may help in finding out more information about the alterations in the nodal properties with regard to TLE. The patients in the current study were investigated pre-operatively and in some cases, there is no definitive diagnosis of laterality of epilepsy. The use of postoperative data, if available, can eliminate this uncertainty.

Conclusion

We identified several differences in graph-based functional connectivity in static and dynamic functional connectivity schemes. We found that using dynamic functional connectivity analysis, the degree centrality and closeness centrality showed greater values, and the clustering coefficient, betweenness centrality, and node neighbor's degree showed smaller values in L-TLE, compared with the R-TLE. Extracting new statistical features from the dynamic graph measures accompanied by the utility of SVM classifiers, more accurate results would be achieved compared with the static analysis. Accounting for the non-stationarity characteristic of the functional connectivity, the graph theoretical measures can be a prerequisite tool in searching for potential connectivity-derived lateralization markers in TLE.

Acknowledgments Authors must recognize and show gratitude towards the prodigious contribution of Iranian National Brain Mapping Laboratory (NBML), Tehran, Iran, for data acquisition service for the entire project.

Funding This work was partially funded and supported by Iran's National Elites Foundation, National Institute for Medical Research Development (Grant No. 971683), and Cognitive Sciences & Technologies Council (Grant No. 6431), between 2017 and 2019.

Compliance with ethical standards

Conflict of interest The authors declare that they have no conflict of interest.

Ethical approval All procedures performed in studies involving human participants were in accordance with the ethical standards of the institutional and/or national research committee and with the 1964 Helsinki declaration and its later amendments or comparable ethical standards.

References

- Berg AT, Vickrey BG, Langfitt JT, Sperling MR, Walczak TS, Shinnar S, Bazil CW, Pacia SV, Spencer SS (2003) The Multicenter Study of Epilepsy Surgery: Recruitment and Selection for Surgery. *Epilepsia*. 44:1425–1433. <https://doi.org/10.1046/j.1528-1157.2003.24203.x>
- Duncan J (1997) Imaging and epilepsy. *Brain*. 120:339–377. <https://doi.org/10.1093/brain/120.2.339>
- Chiang S, Stern JM, Engel J, Levin HS, Haneef Z (2014) Differences in graph theory functional connectivity in left and right temporal lobe epilepsy. *Epilepsy Res* 108:1770–1781. <https://doi.org/10.1016/j.eplepsyres.2014.09.023>
- Jerome E, Murphy GM (2013) NIH Public Access. *Curr Opin Neurol* 36:186–194. <https://doi.org/10.1097/WCO.0b013e32835ee5b8.Connectomics>
- Liao W, Ji G, Xu Q, Wei W, Wang J, Wang Z, Yang F, Sun K, Jiao Q, Richardson MP, Zang Y (2016) Functional Connectome before and following Temporal Lobectomy in Mesial Temporal Lobe Epilepsy. *Nat Publ Group* 6:1–12. <https://doi.org/10.1038/srep23153>
- Cataldi M, Avoli M, De Villers-Sidani E (2013) Resting state networks in temporal lobe epilepsy. *Epilepsia* 54:2048–2059. <https://doi.org/10.1111/epi.12400>
- Sanjari Moghaddam H, Rahmani F, Aarabi MH, Nazem-Zadeh MR, Davoodi-Bojd E, Soltanian-Zadeh H (2019) White matter microstructural differences between right and left mesial temporal lobe epilepsy. *Acta Neurol Belg* 0:0. <https://doi.org/10.1007/s13760-019-01074-x>
- Nazem-Zadeh M-R, Bowyer SM, Moran JE, Davoodi-Bojd E, Zillgitt A, Weiland BJ, Bagher-Ebadian H, Mahmoudi F, Elisevich K, Soltanian-Zadeh H (2016) MEG Coherence and DTI Connectivity in mTLE. *Brain Topogr* 29:598–622. <https://doi.org/10.1007/s10548-016-0488-0>
- Nazem-Zadeh MR, Elisevich K, Air EL, Schwalb JM, Divine G, Kaur M, Wasade VS, Mahmoudi F, Shokri S, Bagher-Ebadian H, Soltanian-Zadeh H (2016) DTI-based response-driven modeling of mTLE laterality. *Neuroimage Clin* 11:694–706. <https://doi.org/10.1016/j.nicl.2015.10.015>
- Su L, An J, Ma Q, Qiu S, Hu D (2015) Influence of resting-state network on lateralization of functional connectivity in mesial temporal lobe epilepsy. *Am J Neuroradiol* 36(8):1479–1487. <https://doi.org/10.3174/ajnr.A4346>
- Karunakaran S, Rollo MJ, Kim K, Johnson JA, Kalamangalam GP, Aazhang B, Tandon N (2018) The interictal mesial temporal lobe epilepsy network. *Epilepsia*. 59:244–258. <https://doi.org/10.1111/epi.13959>
- Gao Y, Zheng J, Li Y, Guo D, Wang M, Cui X, Ye W (2018) Decreased functional connectivity and structural deficit in alertness network with right-sided temporal lobe epilepsy. *Medicine (Baltimore)* 97:1–7. <https://doi.org/10.1097/MD.00000000000010134>
- Dupont S (2002) Bilateral hemispheric alteration of memory processes in right medial temporal lobe epilepsy. *J Neurol Neurosurg Psychiatry* 73:478–485. <https://doi.org/10.1136/jnnp.73.5.478>
- Fallahi A, Nazem-Zadeh M-R, Baniasad F, Lotfi N, Mirbagheri M, Mohammadi-Mobarakeh N, Tapak L, Hashemi-Fesharaki SS, Pooyan M, Mehvari-Habibabadi J (2019) Evolution of Graph Theory in Dynamic Functional Connectivity for Lateralization of Temporal Lobe Epilepsy. In: 2019 41st Annual International Conference of the IEEE Engineering in Medicine and Biology Society (EMBC), IEEE: pp 628–631. <https://doi.org/10.1109/EMBC.2019.8856717>
- Haneef Z, Lenartowicz A, Yeh HJ, Engel J, Stern JM (2012) Effect of lateralized temporal lobe epilepsy on the default mode network. *Epilepsy Behav* 25:350–357. <https://doi.org/10.1016/j.yebeh.2012.07.019>
- Huang DW, Gentili RJ, Reggia JA (2015) Self-organizing maps based on limit cycle attractors. *Neural Netw* 63:208–222. <https://doi.org/10.1016/j.neunet.2014.12.003>
- Vlooswijk MCG, Jansen JFA, Majoie HJM, Hofman PAM, de Krom MCTFM, Aldenkamp AP, Backes WH (2010) Functional connectivity and language impairment in cryptogenic localization-related epilepsy. *Neurology* 75:395–402. <https://doi.org/10.1212/WNL.0b013e3181ebdd3e>

18. Wilke C, Worrell G, He B (2011) Graph analysis of epileptogenic networks in human partial epilepsy. *Epilepsia*. 52:84–93. <https://doi.org/10.1111/j.1528-1167.2010.02785.x>
19. Rubinov M, Sporns O (2010) Complex network measures of brain connectivity: Uses and interpretations. *NeuroImage*. 52:1059–1069. <https://doi.org/10.1016/j.neuroimage.2009.10.003>
20. Bullmore ET, Bassett DS (2011) Brain Graphs: Graphical Models of the Human Brain Connectome. *Annu Rev Clin Psychol* 7:113–140. <https://doi.org/10.1146/annurev-clinpsy-040510-143934>
21. Chang C, Glover GH (2010) Time–frequency dynamics of resting-state brain connectivity measured with fMRI. *NeuroImage*. 50:81–98. <https://doi.org/10.1016/j.neuroimage.2009.12.011>
22. Honey CJ, Sporns O, Cammoun L, Gigandet X, Thiran JP, Meuli R, Hagmann P (2009) Predicting human resting-state functional connectivity from structural connectivity. *Proc Natl Acad Sci* 106:2035–2040. <https://doi.org/10.1073/pnas.0811168106>
23. Ma S, Calhoun VD, Phlypo R, Adalı T (2014) Dynamic changes of spatial functional network connectivity in healthy individuals and schizophrenia patients using independent vector analysis. *NeuroImage*. 90:196–206. <https://doi.org/10.1016/j.neuroimage.2013.12.063>
24. Deco G, Jirsa VK, McIntosh AR (2011) Emerging concepts for the dynamical organization of resting-state activity in the brain. *Nat Rev Neurosci* 12:43–56. <https://doi.org/10.1038/nrn2961>
25. Chiang S, Vankov ER, Yeh HJ, Guindani M, Vannucci M, Haneef Z, Stern JM (2018) Temporal and spectral characteristics of dynamic functional connectivity between resting-state networks reveal information beyond static connectivity. *PLoS One* 13:244976. <https://doi.org/10.1371/journal.pone.0190220>
26. Chai LR, Khambhati AN, Ciric R, Moore TM, Gur RC, Gur RE, Satterthwaite TD, Bassett DS (2017) Evolution of brain network dynamics in neurodevelopment. *Netw Neurosci* 1:14–30. https://doi.org/10.1162/NETN_a_00001
27. Sizemore AE, Bassett DS (2018) Dynamic graph metrics: Tutorial, toolbox, and tale. *NeuroImage*. 180:417–427. <https://doi.org/10.1016/j.neuroimage.2017.06.081>
28. Van Diessen E, Zweiphenning WJEM, Jansen FE (2014) Brain network organization in focal epilepsy : A systematic review and meta-analysis. *PLOS ONE* 9(12):e114606. <https://doi.org/10.1371/journal.pone.0114606>
29. Morgan VL, Abou-Khalil B, Rogers BP (2015) Evolution of Functional Connectivity of Brain Networks and Their Dynamic Interaction in Temporal Lobe Epilepsy. *Brain Connect* 5:35–44. <https://doi.org/10.1089/brain.2014.0251>
30. Yan C-G, Wang X-D, Zuo X-N, Zang Y-F (2016) DPABI: Data Processing & Analysis for (Resting-State) Brain Imaging. *Neuroinformatics*. 14:339–351. <https://doi.org/10.1007/s12021-016-9299-4>
31. Tzourio-Mazoyer N, Landeau B, Papathanassiou D, Crivello F, Etard O, Delcroix N, Mazoyer B, Joliot M (2002) Automated Anatomical Labeling of Activations in SPM Using a Macroscopic Anatomical Parcellation of the MNI MRI Single-Subject Brain. *NeuroImage*. 15:273–289. <https://doi.org/10.1006/nimg.2001.0978>
32. Preti MG, Bolton TAW, Van De Ville D (2017) The dynamic functional connectome: State-of-the-art and perspectives. *NeuroImage* 160:41–54. <https://doi.org/10.1016/j.neuroimage.2016.12.061>
33. Allen EA, Damaraju E, Plis SM, Erhardt EB, Eichele T, Calhoun VD (2014) Tracking whole-brain connectivity dynamics in the resting state. *Cereb Cortex* 24:663–676. <https://doi.org/10.1093/cercor/bhs352>
34. Wang J-H, Zuo X-N, Gohel S, Milham MP, Biswal BB, He Y (2011) Graph Theoretical Analysis of Functional Brain Networks: Test-Retest Evaluation on Short- and Long-Term Resting-State Functional MRI Data. *PLoS One* 6:e21976. <https://doi.org/10.1371/journal.pone.0021976>
35. Quraan MA, McCormick C, Cohn M, Valiante TA, McAndrews MP (2013) Altered Resting State Brain Dynamics in Temporal Lobe Epilepsy Can Be Observed in Spectral Power, Functional Connectivity and Graph Theory Metrics. *PLoS One* 8. <https://doi.org/10.1371/journal.pone.0068609>
36. Liao W, Zhang Z, Pan Z, Mantini D, Ding J, Duan X, Luo C, Lu G, Chen H (2010) Altered functional connectivity and small-world in mesial temporal lobe epilepsy. *PLoS One* 5:27–29. <https://doi.org/10.1371/journal.pone.0008525>
37. Yang Z, Choupan J, Reutens D, Hocking J (2015) Lateralization of temporal lobe epilepsy based on resting-state functional magnetic resonance imaging and machine learning. *Front Neurol* 6:1–9. <https://doi.org/10.3389/fneur.2015.00184>
38. Wu T, Chen D, Chen Q, Zhang R, Zhang W, Li Y, Zhang L, Liu H, Wan S, Jiang T, Zhang J (2018) Automatic Lateralization of Temporal Lobe Epilepsy Based on MEG Network Features Using Support Vector Machines. *Complexity*. 2018:1–10. <https://doi.org/10.1155/2018/4325096>
39. Chiang S, Levin HS, Haneef Z (2015) Computer-automated focus lateralization of temporal lobe epilepsy using fMRI. *J Magn Reson Imaging* 41:1689–1694. <https://doi.org/10.1002/jmri.24696>
40. Farahani N, Fatemizadeh E, Motie Nasrabadi A (2019) Using rDCM method in the mixed model in order to inference effective connectivity in emotions. *Frontiers in Biomedical Technologies* 6(2):106–113. <https://doi.org/10.18502/ftb.v6i2.1692>
41. Van Diessen E, Zweiphenning WJEM, Jansen FE, Stam CJ, Braun KPJ, Otte WM (2014) Brain network organization in focal epilepsy: A systematic review and meta-analysis. *PLoS One* 9. <https://doi.org/10.1371/journal.pone.0114606>
42. Paldino MJ, Golriz F, Chapieski ML, Zhang W, Chu ZD (2017) Brain network architecture and global intelligence in children with focal epilepsy. *Am J Neuroradiol* 38:349–356. <https://doi.org/10.3174/ajnr.A4975>
43. Haneef Z, Chiang S (2014) Clinical correlates of graph theory findings in temporal lobe epilepsy. *Seizure*. 23:809–818. <https://doi.org/10.1016/j.seizure.2014.07.004>
44. Grömping U (2009) Variable Importance Assessment in Regression: Linear Regression versus Random Forest. *Am Stat* 63:308–319. <https://doi.org/10.1198/tast.2009.08199>
45. Farahani FV, Karwowski W, Lighthall NR (2019) Application of graph theory for identifying connectivity patterns in human brain networks: A systematic review. *Front Neurosci* 13:1–27. <https://doi.org/10.3389/fnins.2019.00585>
46. Binnewijzend MAA, Adriaanse SM, Van der Flier WM, Teunissen CE, de Munck JC, Stam CJ, Scheltens P, van Berckel BNM, Barkhof F, Wink AM (2014) Brain network alterations in Alzheimer’s disease measured by Eigenvector centrality in fMRI are related to cognition and CSF biomarkers. *Hum Brain Mapp* 35:2383–2393. <https://doi.org/10.1002/hbm.22335>
47. Lohmann G, Margulies DS, Horstmann A, Pleger B, Lepsien J, Goldhahn D, Schloegl H, Stumvoll M, Villringer A, Turner R (2010) Eigenvector centrality mapping for analyzing connectivity patterns in fMRI data of the human brain. *PLoS One* 5. <https://doi.org/10.1371/journal.pone.0010232>
48. Bernhardt BC, Chen Z, He Y, Evans AC, Bernasconi N (2011) Graph-Theoretical Analysis Reveals Disrupted Small-World Organization of Cortical Thickness Correlation Networks in Temporal Lobe Epilepsy. *Cereb Cortex* 21:2147–2157. <https://doi.org/10.1093/cercor/bhq291>
49. Bartolomei F, Bettus G, Stam CJ, Guye M (2013) Interictal network properties in mesial temporal lobe epilepsy: A graph theoretical study from intracerebral recordings. *Clin Neurophysiol* 124:2345–2353. <https://doi.org/10.1016/j.clinph.2013.06.003>
50. Su L, An J, Ma Q, Qiu S, Hu D (2015) Influence of resting-state network on lateralization of functional connectivity in mesial

- temporal lobe epilepsy. *Am J Neuroradiol* 36:1479–1487. <https://doi.org/10.3174/ajnr.A4346>
51. Rajpoot K, Riaz A, Majeed W, Rajpoot N (2015) Functional connectivity alterations in epilepsy from resting-state functional MRI. *PLoS One* 10:3–5. <https://doi.org/10.1371/journal.pone.0134944>
 52. Coito A, Plomp G, Genetti M, Abela E, Wiest R, Seeck M, Michel CM, Vulliemoz S (2015) Dynamic directed interictal connectivity in left and right temporal lobe epilepsy. *Epilepsia*. 56:207–217. <https://doi.org/10.1111/epi.12904>
 53. Moghaddam HS, Aarabi MH, Mehvari-Habibabadi J, Sharifpour R, Mohajer B, Mohammadi-Mobarakeh N, Hashemi-Fesharaki SS, Elisevich K, Nazem-Zadeh M-R (2020) Distinct patterns of hippocampal subfield volume loss in left and right mesial temporal lobe epilepsy. *Neuro Sci*. <https://doi.org/10.1007/s10072-020-04653-6>
 54. Chiang S, Vankov ER, Yeh HJ, Guindani M, Vannucci M, Haneef Z, Stern JM (2018) Temporal and spectral characteristics of dynamic functional connectivity between resting-state networks reveal information beyond static connectivity. *PLoS One* 13:e0190220. <https://doi.org/10.1371/journal.pone.0190220>
 55. Kaiser RH, Whitfield-Gabrieli S, Dillon DG, Goer F, Beltzer M, Minkel J, Smoski M, Dichter G, Pizzagalli DA (2016) Dynamic Resting-State Functional Connectivity in Major Depression. *Neuropsychopharmacology*. 41:1822–1830. <https://doi.org/10.1038/npp.2015.352>
 56. Chiang S, Cassese A, Guindani M, Vannucci M, Yeh HJ, Haneef Z, Stern JM (2016) Time-dependence of graph theory metrics in functional connectivity analysis. *NeuroImage*. 125:601–615. <https://doi.org/10.1016/j.neuroimage.2015.10.070>
 57. Chiang S, Vankov ER, Yeh HJ, Guindani M, Vannucci M, Haneef Z, Stern JM (2018) Temporal and spectral characteristics of dynamic functional connectivity between resting-state networks reveal information beyond static connectivity. *PLoS One* 13:1–25. <https://doi.org/10.1371/journal.pone.0190220>
 58. Coito A, Genetti M, Pittau F, Iannotti GR, Thomschewski A, Höller Y, Trinka E, Wiest R, Seeck M, Michel CM, Plomp G, Vulliemoz S (2016) Altered directed functional connectivity in temporal lobe epilepsy in the absence of interictal spikes: A high density EEG study. *Epilepsia*. 57:402–411. <https://doi.org/10.1111/epi.13308>
 59. Nazem-Zadeh MR, Elisevich KV, Schwalb JM, Bagher-Ebadian H, Mahmoudi F, Soltanian-Zadeh H (2014) Lateralization of temporal lobe epilepsy by multimodal multinomial hippocampal response-driven models. *J Neurol Sci* 347:107–118. <https://doi.org/10.1016/j.jns.2014.09.029>
 60. Cao X, Qian Z, Xu Q, Shen J, Zhang Z, Lu G (2014) Altered Intrinsic Connectivity Networks in Frontal Lobe Epilepsy: A Resting-State fMRI Study. *Comput Math Methods Med* 2014:1–10. <https://doi.org/10.1155/2014/864979>
 61. Haneef Z, Lenartowicz A, Yeh HJ, Levin HS, Jr JE, Stern JM (2014) Functional connectivity of hippocampal networks in temporal lobe epilepsy. *Epilepsia* 55(1):137–145. <https://doi.org/10.1111/epi.12476>
 62. James GA, Tripathi SP, Ojemann JG, Gross RE, Drane DL (2013) Diminished default mode network recruitment of the hippocampus and parahippocampus in temporal lobe epilepsy. *J Neurosurg* 119:288–300. <https://doi.org/10.3171/2013.3.JNS121041>
 63. Bernasconi N (2003) Mesial temporal damage in temporal lobe epilepsy: a volumetric MRI study of the hippocampus, amygdala and parahippocampal region. *Brain*. 126:462–469. <https://doi.org/10.1093/brain/awg034>
 64. Nazem-Zadeh M-R, Schwalb JM, Elisevich KV, Bagher-Ebadian H, Hamidian H, Akhondi-Asl A-R, Jafari-Khouzani K, Soltanian-Zadeh H (2014) Lateralization of temporal lobe epilepsy using a novel uncertainty analysis of MR diffusion in hippocampus, cingulum, and fornix, and hippocampal volume and FLAIR intensity. *J Neurol Sci* 342:152–161. <https://doi.org/10.1016/j.jns.2014.05.019>
 65. Jafari-Khouzani K, Elisevich K, Wasade VS, Soltanian-Zadeh H (2018) Contribution of Quantitative Amygdalar MR FLAIR Signal Analysis for Lateralization of Mesial Temporal Lobe Epilepsy. *J Neuroimaging* 28:666–675. <https://doi.org/10.1111/jon.12549>

Publisher's note Springer Nature remains neutral with regard to jurisdictional claims in published maps and institutional affiliations.

Affiliations

Alireza Fallahi¹ · Mohammad Pooyan¹ · Nastaran Lotfi² · Fatemeh Baniasad^{3,6} · Leili Tapak^{4,5} · Neda Mohammadi-Mobarakeh^{3,6} · Seyed Sohrab Hashemi-Fesharaki⁷ · Jafar Mehvari-Habibabadi⁸ · Mohammad Reza Ay^{3,6} 

¹ Biomedical Engineering Department, Engineering Faculty, Shahed University, Tehran, Iran

² Departamento de Física, Universidade Federal de Pernambuco, Recife PE 50670-901, Brazil

³ Research Center for Molecular and Cellular Imaging, Advanced Medical Technologies and Equipment Institute (AMTEI), Tehran University of Medical Sciences, Tehran, Iran

⁴ Department of Biostatistics, School of Public Health, Hamadan University of Medical Science, Hamadan, Iran

⁵ Modeling of Noncommunicable Diseases Research Center, Hamadan University of Medical Science, Hamadan, Iran

⁶ Medical Physics and Biomedical Engineering Department, Tehran University of Medical Sciences (TUMS), Tehran, Iran

⁷ Pars Advanced and Minimally Invasive Medical Manners Research Center, Pars Hospital, Iran University of Medical Sciences, Tehran, Iran

⁸ Isfahan Neuroscience Research Center, Isfahan University of Medical Sciences, Isfahan, Iran